



PCCP

**Effects of Applied Surface-tension on Membrane-assisted A $\beta$  Aggregation**

Journal:	<i>Physical Chemistry Chemical Physics</i>
Manuscript ID	CP-ART-06-2021-002642.R2
Article Type:	Paper
Date Submitted by the Author:	24-Aug-2021
Complete List of Authors:	Sahoo, Abhilash; University of Maryland, Fischell Department of Bioengineering Matysiak, Silvina; University of Maryland, Fischell Department of Bioengineering

SCHOLARONE™  
Manuscripts

Cite this: DOI: 00.0000/xxxxxxxxxx

# Effects of Applied Surface-tension on Membrane-assisted A $\beta$ Aggregation<sup>†</sup>

Abhilash Sahoo,<sup>a</sup> and Silvina Matysiak<sup>\*ab</sup>

Received Date

Accepted Date

DOI: 00.0000/xxxxxxxxxx

Accumulation of protein-based (A $\beta$ ) aggregates on cellular membranes with varying structural properties is commonly recognized as the key step in Alzheimer's pathogenesis. But the experimental and computational challenges have made this biophysical characterization difficult. In particular, studies connecting biological membrane organization and A $\beta$  aggregation are limited. While experiments have suggested that an increased membrane curvature results in faster A $\beta$  peptide aggregation in the context of Alzheimer's disease, a mechanistic explanation for this relation is missing. In this work, we are leveraging molecular simulations with a physics-based coarse grained model to address and understand relationships between curved cellular membranes and aggregation of a model template peptide A $\beta$  16-22. In agreement with experimental results, our simulations also suggest a positive correlation between increased peptide aggregation and membrane curvature. More curved membranes have higher lipid packing defects that engage peptide's hydrophobic groups and promote faster diffusion leading to the peptide's fibrillar structures. In addition, we curated the effects of peptide aggregation on membrane's structure and organization. Interfacial peptide aggregation results in heterogeneous headgroup-peptide interactions and an induced crowding effect at the lipid headgroup region, leading to a more ordered headgroup region and disordered lipid-tails at the membrane core. This work presents mechanistic and morphological overview of relationships between biomembrane's local structure and organization, and A $\beta$  peptide aggregation.

## 1 Introduction

Alzheimer's disease is characterized by extracellular self-assembly of A $\beta$  protein segments into ordered fibrillar aggregations<sup>1-3</sup>. Recent reports have pointed to amyloid-membrane interactions as a crucial step in modulating the aggregation kinetics and associated disease pathogenesis<sup>4-7</sup>. In particular, biophysical aspects of membrane organization such as membrane order and charge can affect peptide aggregation kinetics. In addition, peptide aggregation can also effect changes to membrane's structural properties. Three experiment-derived hypothesis detailing effects of peptide aggregation on membrane organization have been suggested — carpeting model, membrane-pore model and detergent model<sup>8</sup>. But the exact biophysical mechanism characterizing this interaction is still missing. While significant research efforts have been applied to understanding peptide aggregation in aqueous solvent, studies in presence of membranous environments are rather lim-

ited. Research in this direction can impact our understanding of event-pathways in Alzheimer's disease.

Recent experimental reports have suggested that A $\beta$  peptide can have differential aggregation patterns when interacting with anionic membranes compared to zwitterionic/cationic ones<sup>9,10</sup>. Here, peptide insertion and peptide aggregation in presence of zwitterionic membranes were correlated to the increased membrane compressibility. Experimental studies have also characterized the dynamic role of membrane curvature in driving the formation of and interaction with amyloids<sup>11,12</sup>. Peptide aggregation was studied with Phosphatidylcholine vesicles of varying sizes using Thioflavin T fluorescence assay to track fibrillation. This study observed a reduced lag time with smaller vesicles compared to larger ones. The authors also used isothermal titration calorimetry to report endothermic binding between A $\beta$  and small lamellar vesicles compared to exothermic binding with large unilamellar vesicles. Such curvature associated modulations in aggregation thermodynamics and kinetics has also been observed in the case of  $\alpha$ -Synuclein (Parkinson's disease) and Huntingtin protein (Huntington's disease), suggesting a fundamental nature in protein aggregate-membrane interactions<sup>13,14</sup>. This presents a need for biophysical studies into membrane curvature driven peptide aggregation.

While increasing molecular simulation studies are focusing on

<sup>a</sup> Biophysics Program, Institute of Physical Science and Technology, University of Maryland, College Park, MD

<sup>b</sup> Fischell Department of Bioengineering, University of Maryland, College Park, MD. E-mail: matysiak@umd.edu

<sup>†</sup> Electronic Supplementary Information (ESI) available: [details of any supplementary information available should be included here]. See DOI: 10.1039/cXCP00000x/

aggregate-membrane interactions, it is difficult to study these processes with traditional all-atom simulations, because of associated long lengths and experimental timescales to study these systems<sup>15–17</sup>. While most studies of membrane-curvature induced peptide behaviour using atomistic simulation have been limited to studies with a single peptide, some emerging work have reported the correlated effects of membrane curvature and peptide aggregation<sup>18,19</sup>. Even atomistic simulations with enhanced sampling approaches are often limited to aqueous solution, considering the increase in quantities and diversities of molecular entities in presence of membranes<sup>20–27</sup>. Another approach that is often applied to address this spatio-temporal scale issue is coarse-graining<sup>28</sup>. This method reduces the resolution of a molecular system by grouping together local atoms, which in turn provides a performance-boost by smoothing the free-energy landscape and preventing locally trapped states. Several coarse-grained models have been applied to study oligomer-membrane associations<sup>29–34</sup>. Physics-based transferable coarse grained forcefields like MARTINI have enabled molecular simulations with exact amino-acid sequences that have coupled protein aggregations to membrane-curvature<sup>35–37</sup>. But MARTINI involves restraining the secondary structure of each protein units, thereby preventing studies of conformational transitions.

In this work, we have used a recently developed a polarizable coarse grained protein and membrane model (Water Explicit Polarizable Coarse-Grained Model — WEPCGM)<sup>38–41</sup>. Our coarse grained protein model captures secondary structural transitions and works in tandem with our membrane model which accurately reproduces membrane electrostatics and structural properties from experiments. Here, we are scoping the study to A $\beta$  16-22 peptide aggregation as this is one of the smallest segment of the full-length peptide that is capable of forming ordered aggregates and has been used as a model template in many experimental and computational investigations<sup>42–45</sup>. Here, we have used 1-palmitoyl-2-oleoyl-sn-glycero-3-phosphocholine (POPC) to create our model lipid membranes, as phosphatidylcholines are the most abundant lipid molecules in mammalian cells and previous experimental studies have used such membranes for peptide-aggregation studies<sup>11</sup>.

## 2 Methods

### 2.1 Coarse Grained Model and Simulation Set-up

Both the membrane and peptide models feature local grouping of atoms to generate functional coarse-grained atom-types (CG-beads) that are representative of the physics and chemistry of the atoms they represent. The molecular polarization is explicitly included by addition of dummy charges on polar coarse-grained sites, such as an amino acid's peptide backbone<sup>46</sup>. These dummy charges on protein and lipid molecules interact with the central CG-bead by harmonic angular potential, and with the local environment through coulombic interactions. Adding explicit-charges to represent dipoles will generate dipole-induced interactions, that can couple environmental fluctuations to protein structure and generate secondary and super-secondary structures. These forcefields have been developed using the polarizable MARTINI

water model<sup>38,39,47</sup>. The protein-backbone and the glycerol-esters are modeled as polarizable beads in the case of peptides and lipid molecules, respectively. Beads representative of lipid tails and hydrophobic residue sidechains, are modeled as hydrophobic beads. Some of the beads representing parts of lysine and glutamate sidechains have explicit charges to represent cationic and anionic nature of the respective amino acids. A more explicit description of the forcefield is presented in the supplementary information (Fig. S1, S2). Previous reports have explored the use of these CG models to study membrane-induced peptide folding, calcium ion driven lipid demixing and peptide aggregation in presence of membranes<sup>38–41,45</sup>. Recently, we validated our forcefield by simulations with A $\beta$  16-22 peptide in aqueous solution and in presence of membranes composed of POPC and POPS lipids, where peptides were allowed to interact with the membrane from solution and form ordered aggregates<sup>45</sup>.

Similar to Terakawa *et al.*'s experimental study on the effect of membrane-curvature on peptide aggregation, our model lipid membranes are also composed of POPC lipids<sup>11</sup>. The initial frame was prepared with A $\beta$  16-22 peptides (with peptide to lipid ratio of 1:10, similar to experimental systems outlined in Kandel *et al.*<sup>48</sup>) solvated randomly away from the membrane. We instituted a hardcore repulsion with  $c_6$  and  $c_{12}$  terms set to 0 and 0.00247 respectively between lipid headgroups (phosphate and choline) in the lower leaflet and the peptide backbone. This forces the peptides to exclusively interact with the upper leaflet. As previous simulations have shown that this peptide fragment primarily stays at the membrane-water interface, such applied repulsion between the lower leaflet and the peptide backbone would not affect the peptide aggregation and adsorption properties. Each simulation system was composed with 242 POPC lipid molecules, 24 A $\beta$  16-22 peptides solvated in 5400 coarse grained water molecules. The membranes were held with different values of surface-tension to reproduce conditions with varying curvature. Such an approach of using applied surface-tension as proxies for membrane curvature has been previously used in atomistic simulations to study membrane insertion of anti-microbial peptides<sup>49</sup>. Furthermore, A $\beta$  16-22 stays at the membrane-interface, where membrane-curvature primarily manifests as an increased area-per-lipid<sup>45</sup>. Fig. 1 shows the relationship between the area-per-lipid and the applied surface-tension values in standalone simulations with POPC membranes in absence of peptides. The area per lipid is computed simply by dividing the total membrane lateral area with the number of lipid molecules in one leaflet. The highest surface-tension in our case corresponds to a small unilamellar vesicle with a diameter of 13.4 nm, which was verified with a 100 ns molecular simulation of complete vesicle (877 lipids)<sup>45</sup>. These values are similar to those reported with coarse-grained and large all-atom simulations<sup>50–52</sup>. We also simulated a larger membrane with 512 POPC lipid molecules, 50 A $\beta$  16-22 peptides and 9973 coarse-grained water molecules at the highest value of surface-tension for 1.5 microseconds, to verify that our system does not suffer from finite size effects.

The simulation protocol is identical to that mentioned in Sahoo *et al.*<sup>45</sup>. A brief overview is presented here. The initial

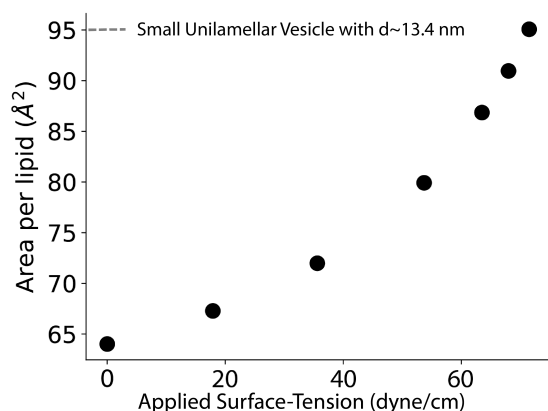


**Fig. 1** Relationship between applied surface-tension and the area-per-lipid. Each point denotes a simulation system.

peptide-membrane system was created with peptides dispersed randomly in solution, away from the membrane. The molecular system was then energy minimized and equilibrated for a period of 50 nanoseconds, with position restraints on the peptides. After that, the position restraints were removed and the peptides were allowed to interact among themselves and with the membrane during the production phase of 1.5 microseconds. All the simulations were performed with GROMACS 4.5.7<sup>53</sup>, with temperature maintained at 300K with a Nosé-Hoover thermostat<sup>54</sup> and pressure by Berendsen barostat<sup>55</sup>. Two independent replicas were simulated for each simulation condition. The long range electrostatics is determined through Particle-Mesh Ewald method with relative dielectric constant of 2.5.

## 2.2 Analysis

We have used visual molecular dynamics<sup>56</sup> and in-house developed scripts to analyze our molecular simulations. Different geometric features of peptide and lipid organization was used to define peptide absorption and ordered aggregation. We used the position of two second sidechain beads (S2) of PHE to determine absorption of a peptide into the membrane. First, six nearest lipid phosphate groups closest to the peptide center-of-mass were used to create a local membrane plane for each peptide, thereby allowing accommodations for local membrane undulations. Then, peptides were classified as absorbed if at least one of the PHE-S2 of the peptides moved beyond that local plane in the z-direction. Here, we classified peptide aggregates as "ordered" if each peptide in that aggregate participates in at least three backbone-driven dipole orientations (Fig. S3). Such dipole-dipole interactions can be construed as equivalent to hydrogen bonds (as observed in atomistic representation of a  $\beta$  sheet) in a coarse-grained sense.

## 3 Results and Discussion

### 3.1 Impact of induced curvature on peptide aggregation

To determine the effect of membrane curvature on peptide aggregation, we characterized the structure of peptide aggregates in simulation with varying applied surface-tension values. Fig. 2 records the overall behavior (in-solution + on-membrane) of pep-

ptide aggregates, with measures for total ordered-aggregate fraction (Fig. 2a) and ordered-aggregate fraction among the peptides absorbed on the membrane (Fig. 2b). Peptides can interact and aggregate both in solution and on top of membranes. This competition between peptide-peptide and peptide-membrane interaction shapes the peptide aggregation behavior. At surface-tension values greater than 35 dyne/cm, peptide absorption progressively increases. This increase in peptide absorption, in turn leads to an increased arrangement of the absorbed peptides into ordered macro-structures on the membrane surface (Fig. 2b), which increases the overall ordered content. It is worth noting that such increased fibrillation in more-curved membranes are in line with experimental observation of increased beta-sheets in small unilamellar vesicles compared to larger ones<sup>11</sup>. The computed fraction of absorbed peptides (1.0) and fraction of total ordered aggregation (0.68, standard deviation 0.02) from a larger simulation system at the highest surface-tension agrees with the values from the smaller system, suggesting no finite size effects. Therefore all further analyses presented in this article have focused on the smaller peptide-membrane systems.

To understand of this curvature-induced peptide fibrillation, we used geometric and physical metrics that quantify membrane's structure and organization. Fig. 3a shows the distribution of hydrophobic solvent-accessible-surface-area (HSASA) for membranes at different values of surface-tension. An increased HSASA is indicative of more hydrophobic defects that can affect membrane-peptide interactions. These evidences suggest, peptide absorption is driven by increased hydrophobic defects in membranes with higher surface-tension. This is apparent in the molecular snapshot (Fig. 3b) showing these peptide aggregations on top of an exposed hydrophobic patch of the membrane at the highest surface-tension. Furthermore, increased area compressibility of these membranes allow for easy rearrangement of lipid molecules to sustain larger absorbed aggregates. Also, due to reduced crowding, peptide diffusion is faster in membranes with higher surface-tension (Fig. S4). Now, as we are working with a dominantly hydrophobic fragment of the A $\beta$  peptide, the hydrophobic side-chains of the absorbed peptides primarily interact with the membrane's acyl core. With increasing surface-tension values, these absorbed peptides with their side-chains engaged can diffuse around faster. The interaction between the peptides are then driven by backbone dipole alignments leading to ordered beta-sheet like structures. A parallel with glycine-valine repeats at hexadecane-water interface can be drawn here, with fibrillation at the interface region driven by buried hydrophobic sidechains into apolar media<sup>46</sup>. Therefore, this increased fibrillation fraction at later surface-tension values can be attributed to the cumulative effects of peptide absorption, higher membrane compressibility and faster peptide diffusion. It is worth noting here that similar to earlier solid-state NMR experiments, our simulations also report some ordered aggregations into cross-beta like structures in solution phase on membranes with lower surface-tension values (Fig. 3 - c, d)<sup>42</sup>. Here the peptide aggregates primarily in solution, tethered to the membrane (Fig. 3c). Such cross-beta structures are also noted for our simulations in solution, in absence of any membranes (Fig. S5). But, the prevalence of ordered ag-

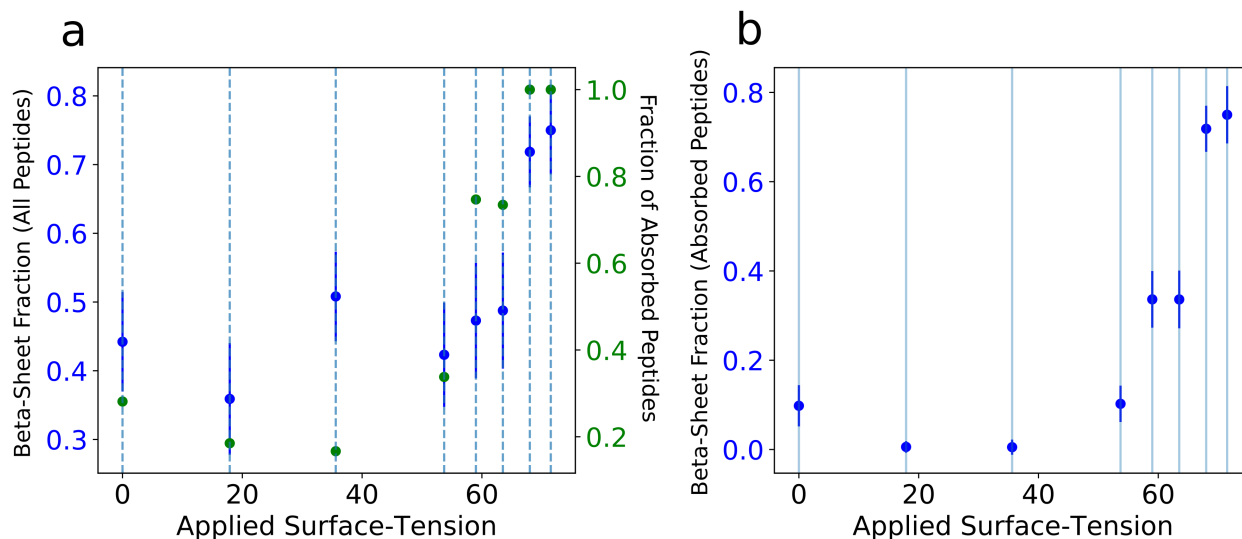


**Fig. 2** Variation of peptide absorption and ordered aggregation with increasing surface-tension. a) Absorption (Green) and ordered aggregation (Blue) among all the peptides (in-solution + on-membrane). b) Ordered aggregation (Blue) among peptides absorbed on the membrane only. These values are averaged over the last 200 nanoseconds of two independent replicates.

gregation is higher on "more curved" membranes because of the specific topological aspects (hydrophobic defects) that promote more absorption and backbone-driven inter-peptide interactions.

### 3.2 Effects of peptide aggregation on membrane structure

Amyloid depositions can alternatively affect membrane's structure which can in turn result in functional changes. Several studies have reported A $\beta$  assisted membrane damage with formation of heterogeneous pores or detergent-like effects<sup>7</sup>. A correlation between membrane fluidity and A $\beta$  self-assembly was suggested in experiments using dynamic light scattering, fluorescence and electron microscopy techniques<sup>57</sup>. This disruption of membranous environments is also noted by Lemkul *et al.* for single A $\beta$  peptide with atomistic simulations<sup>58</sup>. The authors reported several structural impacts of A $\beta$ -membrane interactions including local disordering of lipid groups, and increased tail-tilts.

In this work, we also analyzed induced changes in membrane order and headgroup tilt due to peptide aggregation. While the reported behavior exist in all simulation systems, we have shown results from membranes with the highest surface-tension as that system has the highest number of absorbed peptides, and therefore can be used to report statistically significant results. The coarse-grained tail order parameter,  $\frac{1}{2}(3\langle\cos^2\theta\rangle - 1)$ , quantifies disorder in acyl tails. Here  $\theta$  is the angle made by each bond vector in the acyl tail with the bilayer normal. The order parameter varies from -0.5 to 1, reaching the maximum value when bond vectors are aligned parallel to membrane normal. We classified lipid molecules in contact (any CG-bead within 7 angstroms) from the peptide aggregate as "close-to-aggregate" and others as "away-from-aggregate". Fig. 4a reports the tail order parameter at the interaction-sites of the acyl tail starting from the region near the headgroups to the center of the membrane. As compared to lipid molecules that are away from the aggregate, the lipid molecules closer to the aggregate are more ordered at the

interfacial region, and more disordered deeper inside the membrane. This observation can be explained in terms of the location of the peptide aggregate along the Z-axis (Fig. 4b). Due to the presence of peptide aggregates, the interfacial regions get more crowded, inducing increased order closer to the aggregates (Fig. 4a). Farther inside the membrane, a hollow defect is generated by pushing the headgroups away at the interface (Fig. 4b), which contributes to more disorder near the bilayer center, closer to the aggregates. These observations align with the reported "aggregate induced order" in previous-mentioned experimental study<sup>57</sup>. We observed this order at the interfacial region, and a more disordered acyl tail inside the membrane core as the short peptides reside at the membrane interface.

Finally, we also looked at how the lipid headgroups behave closer to the aggregate as compared to away from it. Differential arrangement of lipid headgroups can alter local membrane potential and have implications in cellular signalling processes. The distribution of headgroup ( $\vec{P}\vec{N}$ ) tilt with respect to the bilayer normal is plotted in Fig 4c.  $\vec{P}\vec{N}$  tilt is more dispersed closer to the aggregate. This can be understood in terms of increased heterogeneity induced by peptide-lipid interactions at the headgroups, closer to the aggregate.

## 4 Conclusions

Peptide aggregation into structured deposits have been associated with many neurodegenerative diseases, particularly through interaction with cellular membranes. Experimental results have suggested that both membranes and peptide can influence each other's structure and dynamics. Membrane curvature can promote extensive fibrillation, with faster formation of ordered structures in presence of small unilamellar vesicles, compared to larger ones. On the other hand, peptide aggregates can alter membrane's structure and packing. In this work we have investigated these intertwined effects with coarse-grained molecular simula-

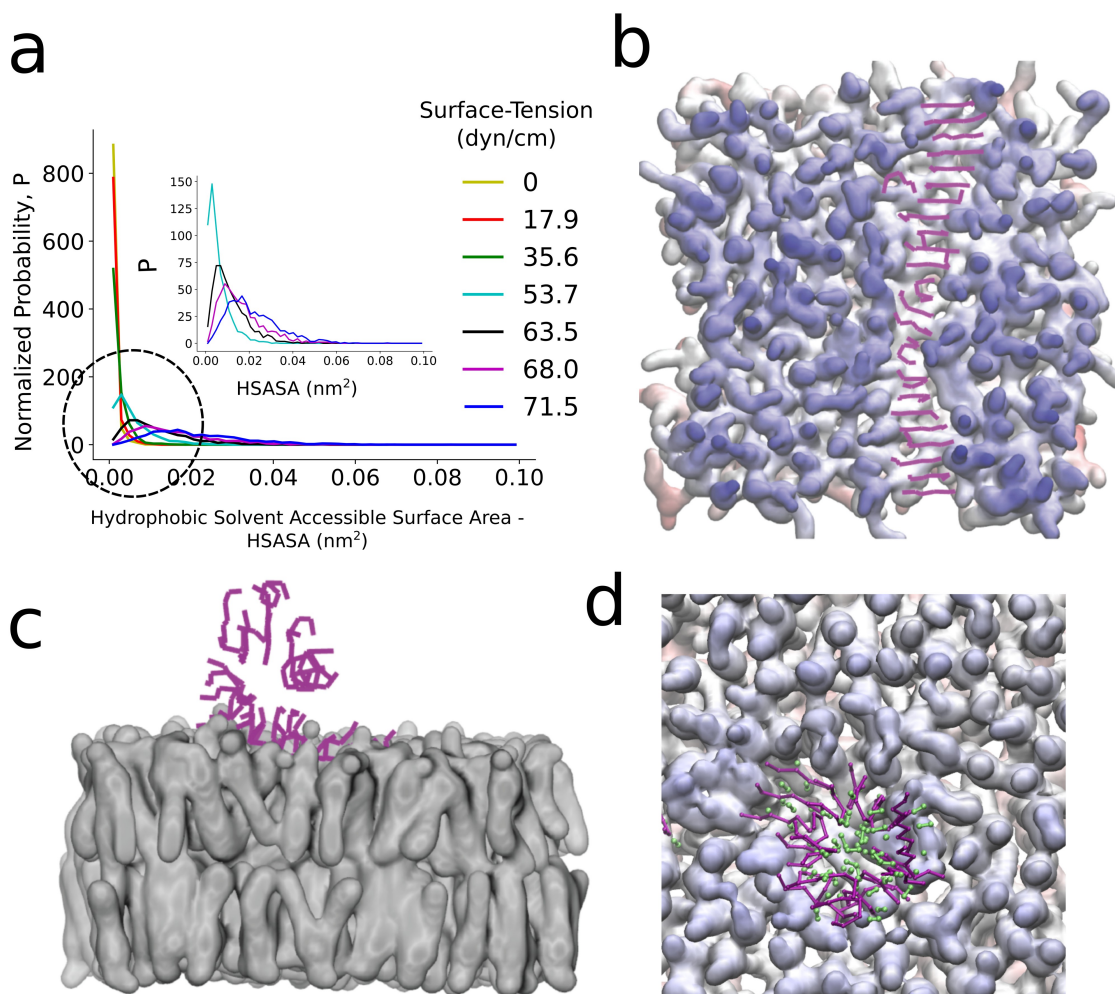


**Fig. 3** (a) Hydrophobic solvent accessible surface-area of membranes in absence of peptides. Snapshots of membranes with peptide aggregate. b - Simulation with surface-tension of 71.5 dyne/cm. Coloring Scheme - Membrane components are colored by their position along Z, from red to blue; Peptides: Magenta. c - Simulation without surface-tension (Lateral view). Coloring scheme - Membranes: Grey. d - Simulation without surface-tension (Top view). Coloring Scheme - Membrane components are colored by their position along Z, from red to blue; Peptides: Magenta; Hydrophobic groups: Lime

tions. Our results agree with previous observations of curvature-driven peptide aggregation into ordered structures, and suggest possible biophysical mechanisms for it<sup>11,12</sup>. Membranes with increased curvatures lead to increased peptide absorption, due to more exposed hydrophobic defects. The absorbed peptides can then laterally diffuse around, and interact through the peptide backbone to form ordered fibrillar structures. The presence of such peptide aggregates also affects the lipid membrane's local structure. The lipid groups closer to the aggregates are more ordered at the crowded interfacial region due to interfacial presence of peptides; and less ordered deep inside the membrane core. These observations align with previous experiments and molecular simulations that also highlighted membrane disruption by peptides<sup>57,58</sup>. Our results support the previously suggested "carpeting model" of membrane disruption, by increasing membrane fluidity inside the membrane core<sup>7,59</sup>. These locally close lipids also have a broad distribution in  $\vec{P}\vec{N}$  vector tilt from the membrane normal, suggesting the heterogeneous nature of

peptide-lipid interactions. Such local variations in  $\vec{P}\vec{N}$  vector tilt can manifest in changes to the membrane's electrostatic potential, ion distributions and alter electrostatics-assisted membrane signalling<sup>60,61</sup>. This study unravels the effects of membrane curvature in aiding peptide aggregation, and the effects of peptide aggregation in reshaping membrane's local attributes.

## Conflicts of interest

There are no conflicts to declare.

## Acknowledgements

This research was supported by the National Science Foundation under the Grant CHE-1454948 (A.S. and S.M.), DGE-1632976 (A.S.), and through computing resources provided by the University of Maryland and Texas Advanced Computing Center - TACC (TG-MCB120045).

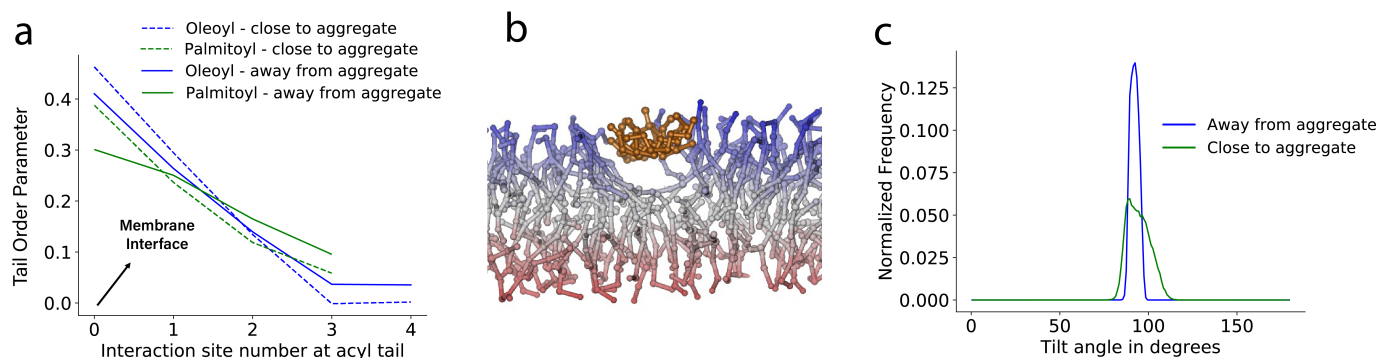


**Fig. 4** a - Lipid tail order with respect to interaction site at acyl tail, numbered starting from the membrane interface. b - A snapshot of peptide aggregate on the membrane for simulation with surface-tension of 71.5 dyne/cm. Coloring Scheme - Membrane components are colored by their position along Z, from red to blue; Peptides: Orange. c - Distribution of headgroup (PN-vector) tilt with-respect-to the bilayer normal.

## Notes and references

- G. G. Glenner and C. W. Wong, *Biochem. Biophys. Res. Commun.*, 1984, **122**, 1131–1135.
- G. G. Glenner and C. W. Wong, *Biochem. Biophys. Res. Commun.*, 1984, **120**, 885–890.
- C. L. Masters, G. Simms, N. A. Weinman, G. Multhaup, B. L. McDonald and K. Beyreuther, *Proc. Natl. Acad. Sci. U.S.A.*, 1985, **82**, 4245–9.
- M. P. Murphy and H. I. LeVine, *J. Alzheimers Dis.*, 2010, **19**, 311–323.
- E. Drolle, A. Negoda, K. Hammond, E. Pavlov and Z. Leonenko, *PLoS ONE*, 2017, **12**, e0182194.
- K. Matsuzaki, *Biochim. Biophys. Acta, Biomembr.*, 2007, **1768**, 1935–1942.
- A. Sahoo and S. Matysiak, *Phys. Chem. Chem. Phys.*, 2019, **21**, 22679–22694.
- K. Berthelot, C. Cullin and S. Lecomte, *Biochimie*, 2013, **95**, 12–19.
- N. Sureshbabu, R. Kirubakaran, H. Thangarajah, E. J. P. Malar and R. Jayakumar, *J. Mol. Neurosci.*, 2010, **41**, 368–382.
- F. Hane, E. Drolle, R. Gaikwad, E. Faught and Z. Leonenko, *J. Alzheimers Dis.*, 2011, **26**, 485–494.
- M. S. Terakawa, Y. Lin, M. Kinoshita, S. Kanemura, D. Itoh, T. Sugiki, M. Okumura and Y.-H. Lee, *Biochim. Biophys. Acta, Biomembr.*, 2018, **1860**, 1741–1764.
- Y. Sugiura, K. Ikeda and M. Nakano, *Langmuir*, 2015, **31**, 11549–11557.
- I. M. Pranke, V. Morello, J. Bigay, K. Gibson, J.-M. Verbavatz, B. Antonny and C. L. Jackson, *J. Cell Biol.*, 2011, **194**, 89.
- M. Chaibva, K. A. Burke and J. Legleiter, *Biochemistry*, 2014, **53**, 2355–2365.
- L. Thøgersen, B. Schjøtt, T. Vosegaard, N. C. Nielsen and E. Tajkhorshid, *Biophys. J.*, 2008, **95**, 4337–4347.
- A. M. Brown and D. R. Bevan, *Biophys. J.*, 2016, **111**, 937–949.
- L. N. Zhao, S.-W. Chiu, J. Benoit, L. Y. Chew and Y. Mu, *J. Phys. Chem. B*, 2011, **115**, 12247–12256.
- G. C. A. d. Hora, N. L. Archilha, J. L. S. Lopes, D. M. Müller, K. Coutinho, R. Itri and T. A. Soares, *Soft Matter*, 2016, **12**, 8884–8898.
- D. E. S. Santos, L. Pol-Fachin, R. D. Lins and T. A. Soares, *J. Chem. Inf. Model*, 2017, **57**, 2181–2193.
- R. Wu, J. Liu, X. Qiu and M. Deng, *Mol Simul*, 2017, **43**, 1227–1239.
- B. Urbanc, L. Cruz, F. Ding, D. Sammond, S. Khare, S. Buldyrev, H. Stanley and N. Dokholyan, *Biophys. J.*, 2004, **87**, 2310–2321.
- M. Biancalana and S. Koide, *Biochim. Biophys. Acta, Proteins Proteomics*, 2010, **1804**, 1405–1412.
- N. G. Sgourakis, M. Merced-Serrano, C. Boutsidis, P. Drineas, Z. Du, C. Wang and A. E. Garcia, *J. Mol. Biol.*, 2011, **405**, 570–583.
- N. G. Sgourakis, Y. Yan, S. A. McCallum, C. Wang and A. E. Garcia, *J. Mol. Biol.*, 2007, **368**, 1448–1457.
- N. Nishikawa, P. H. Nguyen, P. Derreumaux and Y. Okamoto, *Mol Simul*, 2015, **41**, 1041–1044.
- D. K. Klimov and D. Thirumalai, *Structure*, 2003, **11**, 295–307.
- S. Santini, N. Mousseau and P. Derreumaux, *J. Am. Chem. Soc.*, 2004, **126**, 11509–11516.
- S. Kmiecik, D. Gront, M. Kolinski, L. Wieteska, A. E. Dawid and A. Kolinski, *Chem. Rev.*, 2016, **116**, 7898–7936.
- S. Abeln, M. Vendruscolo, C. M. Dobson and D. Frenkel, *PLoS ONE*, 2014, **9**, e85185.
- R. Friedman, R. Pellarin and A. Caflich, *J. Mol. Biol.*, 2009, **387**, 407–415.
- A. Morriss-Andrews, F. L. H. Brown and J.-E. Shea, *J. Phys. Chem. B*, 2014, **118**, 8420–8432.
- M. Chiricotto, T. T. Tran, P. H. Nguyen, S. Melchionna, F. Sterpone and P. Derreumaux, *Isr. J. Chem.*, 2017, **57**, 564–573.
- Y. Chebaro, S. Pasquali and P. Derreumaux, *J. Phys. Chem. B*, 2012, **116**, 8741–8752.
- M. Cheon, I. Chang and C. K. Hall, *Proteins*, 2010, **78**, 2950–2960.
- S. J. Marrink, H. J. Risselada, S. Yefimov, D. P. Tieleman and

- A. H. de Vries, *J. Phys. Chem. B*, 2007.
- 36 F. Elías-Wolff, M. Lindén, A. P. Lyubartsev and E. G. Brandt, *Soft Matter*, 2019, **15**, 792–802.
- 37 J. Gómez-Llobregat, F. Elías-Wolff and M. Lindén, *Biophys. J.*, 2016, **110**, 197–204.
- 38 S. J. Ganesan and S. Matysiak, *Phys. Chem. Chem. Phys.*, 2016, **18**, 2449–2458.
- 39 S. J. Ganesan, H. Xu and S. Matysiak, *J. Phys. Chem. B*, 2017, **121**, 787–799.
- 40 S. J. Ganesan, H. Xu and S. Matysiak, *Phys. Chem. Chem. Phys.*, 2016, **18**, 17836–17850.
- 41 A. Sahoo and S. Matysiak, *J. Phys. Chem. B*, 2020, **124**, 7327–7335.
- 42 J. J. Balbach, Y. Ishii, O. N. Antzutkin, R. D. Leapman, N. W. Rizzo, F. Dyda, J. Reed and R. Tycko, *Biochemistry*, 2000, **39**, 13748–13759.
- 43 K. Kowalski and N. P. Bauman, *J. Chem. Phys.*, 2020, **153**, 049902.
- 44 X. Ge, Y. Sun and F. Ding, *Biochim Biophys Acta Biomembr*, 2018, **1860**, 1687–1697.
- 45 A. Sahoo, H. Xu and S. Matysiak, *Phys. Chem. Chem. Phys.*, 2019, **21**, 8559–8568.
- 46 S. J. Ganesan and S. Matysiak, *J. Chem. Theory Comput.*, 2014, **10**, 2569–2576.
- 47 S. O. Yesylevskyy, L. V. Schäfer, D. Sengupta and S. J. Marrink, *PLOS Comput. Biol.*, 2010, **6**, e1000810.
- 48 N. Kandel, T. Zheng, Q. Huo and S. A. Tatulian, *J. Phys. Chem. B*, 2017, **121**, 10293–10305.
- 49 K. A. Reid, C. M. Davis, R. B. Dyer and J. T. Kindt, *Biochim Biophys Acta Biomembr*, 2018, **1860**, 792–800.
- 50 S. O. Yesylevskyy, T. Rivel and C. Ramseyer, *Sci. Rep.*, 2017, **7**, 16078.
- 51 S. J. Marrink and A. E. Mark, *J. Chem. Phys.*, 2003.
- 52 C.-M. Lin, C.-S. Li, Y.-J. Sheng, D. T. Wu and H.-K. Tsao, *Langmuir*, 2012, **28**, 689–700.
- 53 M. J. Abraham, T. Murtola, R. Schulz, S. Páll, J. C. Smith, B. Hess and E. Lindahl, *SoftwareX*, 2015, **1-2**, 19–25.
- 54 S. Nosé, *Mol. Phys.*, 1984, **52**, 255–268.
- 55 H. J. C. Berendsen, J. P. M. Postma, W. F. van Gunsteren, A. DiNola and J. R. Haak, *J. Chem. Phys.*, 1984, **81**, 3684–3690.
- 56 W. Humphrey, A. Dalke and K. Schulten, *J Mol Graph*, 1996, **14**, 33–38.
- 57 M. F. Sciacca, C. Tempra, F. Scollo, D. Milardi and C. La Rosa, *Biochim Biophys Acta Biomembr*, 2018, **1860**, 1625–1638.
- 58 J. A. Lemkul and D. R. Bevan, *FEBS J.*, 2009, **276**, 3060–3075.
- 59 T. L. Williams and L. C. Serpell, *FEBS J.*, 2011, **278**, 3905–3917.
- 60 X. Lin, V. Nair, Y. Zhou and A. A. Gorfe, *Phys. Chem. Chem. Phys.*, 2018, **20**, 15841–15851.
- 61 C.-J. Högberg and A. P. Lyubartsev, *Biophys. J.*, 2008, **94**, 525–531.